CHAPTER 7

Soft X-ray Absorption Methods

A. Knop-Gericke[1], F. M. F. de Groot[2], J. A. van Bokhoven[3], T. Ressler[1]

[1]Fritz-Haber-Institut der MPG, Department of Inorganic Chemistry, Faradayweg 4-6, 14195 Berlin, Germany

[2]Department of Inorganic Chemistry and Catalysis, Utrecht University, Sorbonnelaan 16, 3508 TB Utrecht, The Netherlands

[3]Laboratory for Technical Chemistry, ETH Hönggerberg, CH-8093 Zurich, Switzerland

Abstract

The application of *in-situ* X-ray absorption spectroscopy in the soft energy range for the investigation of heterogeneous catalytic processes is discussed. The design of *in-situ* cells is described and the data analysis regarding the subtraction the gas phase signal is discussed. Five examples of *in-situ* X-ray absorption measurements are presented. Two of these studies correlate the electronic structure of the catalyst surface with the catalytic activity. Alternative methods, including soft XAS using fluorescence detection and X-ray raman detection of soft XAS, which have the potential to be applied for *in-situ* studies on working catalyst surfaces, are also discussed.

CONTENTS

Email: f.m.f.degroot@chem.uu.nl

ISBN: 0-00000-000-0/$25.00

PREFACE

X-ray absorption spectroscopy represents a powerful method for the investigation of the electronic and geometric structure of catalysts. Information concerning the catalyst surface can be revealed by applying X-ray absorption spectroscopy in the soft energy range. X-ray absorption spectroscopy in the soft energy range is usually applied under ultra high vacuum conditions because of the strong absorption of soft X-ray radiation in gas. Many X-ray absorption studies in the soft energy range at room temperature, or at liquid nitrogen temperature performed under UHV conditions on heterogeneous catalysts, were published. Results obtained from these investigations do not necessarily reflect the structure of a working catalyst because the structure of the catalyst surface in vacuum might be different from the surface structure of the catalyst under reaction conditions. Nonetheless, these investigations revealed many interesting details about the surface of catalysts. These studies do have critical disadvantages, since the results obtained under ultra high vacuum conditions might not be transferred to real catalytic conditions with reaction atmospheres of at least one bar. This phenomenon is called "pressure gap" in the research of heterogeneous catalytic processes.

Therefore, much attention is given to transfer the method to catalytically more relevant conditions and to bridge the pressure and material gaps. First efforts in this direction have been made by coupling a reactor, in which heterogeneous catalytic processes under high-pressure conditions were performed, using a sample transfer system with a chamber that allows measuring X-ray absorption spectra under UHV-conditions. However, thismehtod of detecting X-ray absorption spectra in the soft energy range is not a true *in-situ* measurement since it requires interrupting the catalytic reaction. A real *in-situ* measurement facilitates the simultaneous detection of physical and/or chemical properties of the catalyst and the performance of the catalyst in the heterogeneous catalytic reaction.

Within the last few years, reactor cells have been developed that allow the detection of X-ray absorption spectra in the energy range 300 eV$\leq$h$\nu\leq$2500 eV under reaction conditions. These cells offer the possibility to measure the catalytic activity and the electronic structure of the active catalyst surface simultaneously. Two different types of cells have been reported for *in-situ* investigations in the soft energy range. One type is used in the energy range 1000$\leq$h$\nu\leq$3500 eV. It can be operated at 1 bar. *In-situ* measurements on elements heavier than potassium are standard within the experimental set-up. The unwanted absorption of radiation by the elements and the air is very significant for the lighter elements with edges of energies $<$2.5 keV. The transmission of an X-ray beam through 20 cm of air is significantly suppressed at energies lower than 2.5 keV (see Fig. 1).

The other type of cell, which operates at lower energies in the range 150 eV$\leq$ h$\nu\leq$ 1000 eV can be operated at mbar pressure only because of the strong absorption of X-ray radiation below 1000eV.

1. SOFT X-RAY *IN-SITU* CELLS

In this paragraph, two types of soft X-ray *in-situ* cells will be introduced. The cells allow the detection of X-ray absorption spectra of working catalyst surfaces. Since heterogeneous catalytic processes take place at the surface of a catalyst, it is a crucial requirement for the understanding of these reactions to determine the electronic surface structure of active catalyst surface. X-ray absorption spectroscopy in the soft energy range is usually applied on single crystals under ultra high vacuum (UHV) conditions. Catalytic relevant systems are powders that are used in reactions at atmospheric or even higher pressures. Therefore, the transfer of results achieved from UHV studies on single crystals to real catalytic systems is obstructed by the so-called pressure and material gap. The surface sensitivity of soft X-rays facilitates the investigation of light elements, like carbon or oxygen, on the surface. The complexity of *in-situ* X-ray absorption investigations in the soft energy range is higher compared to *in-situ* X-ray absorption studies in the hard X-ray range. A high photon transmission in the soft energy range, vacuum pumps and special gas phase detectors, offered by special X-ray windows, are required as described below. The volume structure of a working catalyst can be estimated by X-ray absorption spectroscopy in the hard energy range (see the chapter on hard X-ray absorption spectroscopy). The bulk sensitivity of this radiation and the possibility to detect time resolved spectra with high time resolution facilitates the investigation of solid state dynamics. The interaction between the surface and the volume of a working catalyst that is postulated in the Mars-van-Krevelen-Mechanism requires both the electronic structure of the working catalyst surface and the volume structure of the active catalyst. A complete description of the working catalyst can be

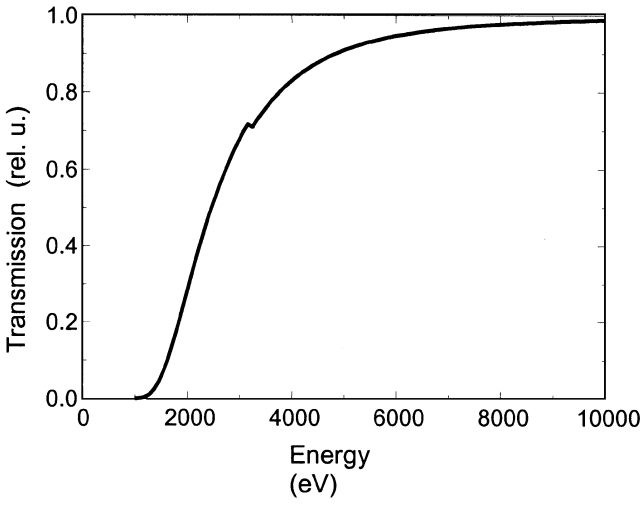

Figure 1. Calculated X-ray transmission of 20 cm air as a function of X-ray energy.

achieved only by a combination of *in-situ* hard X-ray studies to detect the bulk properties and *in-situ* soft X-ray studies providing information on the electronic surface structure.

1.1. The Energy Range 1000–3500 eV

An apparatus working in the range from 1000–3500 eV is described in the literature [1]. The apparatus can be used for *in-situ* investigation in a pressure range of $10^{-4} < p < 1$ bar and a temperature range of 80 K $< T <$ 750 K. Pre-treatment in the gas atmospheres of 5 bar and temperatures up to 750 K can be performed in the same cell. The modular setup allows the application of different detector systems like high sensitive fluorescence and electron yield detectors.

The apparatus developed by Bokhoven et al. in Utrecht University consists of a vacuum chamber, the *in-situ* cell inside the vacuum chamber, and several high sensitive fluorescence and electron yield detectors. The chamber is a cross of 80 cm × 90 cm using a CF 250 flange to connect the apparatus to the beamline as shown in Fig. 2. A base pressure of better than 10^{-6} mbar is achieved. The chamber is adjustable in *x*, *y*, *z*-direction to realize an accurate alignment to the X-ray beam. The *in-situ* cell is mounted onto a manipulator, which allows precise positioning of the *in-situ* cell in the X-ray beam. Additional linear manipulators are installed in front and behind the *in-situ* cell. The manipulator in front of the sample is equipped by a gold and copper mesh and by a phosphorous screen. The meshes are used to measure the intensity of the initial beam (I_0 signal) and the screen enables the alignment of the vacuum chamber. The second foil holder can be used to measure the reflection EXAFS or other signals. A slit holder is mounted on an additional manipulator that is installed on flange D. By rotation of this manipulator, the beam spot can be reduced to any size. The vertical tube provides eight flanges (CF63) denoted as A in Fig. 2 for electrical and gas feed through. Flexible metal tubes transport the gases to the in-stu cell and to the fluorescence detector (gas proportional counter). Electrical feed throughs for power supplies or pre-amplifiers, furnace and IR lamps, and thermocouples are also attached to the chamber. In addition, the vacuum chamber has six viewports (C), which are very helpful for the alignment of the chamber. Moreover, to view the interior of the chamber, a leaded window is mounted at the end of the horizontal tube and in the front door. The front door is also used to place and replace the *in-situ* cell. The *in-situ* cell consists of three parts as shown in Fig. 3. A represents a stainless steel cube with window holders. The holders (W_1 and W_2) are mounted at a 90° angle, and hold entrance and exit windows, respectively. A gas proportional counter or photo diode is integrated into the exit window. The window holders ($W_{3)}$ are blank. The entrance port has a 7μm thick gas-tight beryllium window (13mm diameter) fixed to a support with an aperture of 12 × 8 mm. The window is not transparent for visible light. The exit window consists of a 13 μm thick beryllium window with a diameter of 23 mm, which is mounted on a support with an aperture of 22 mm. This window withstands a pressure difference of 1 bar. The window holders are equipped with PTFE o-rings on the side in the cube, which position the reaction chamber of the *in-situ* cell like a ball valve. The reaction chamber, which is a sphere welded on a flange, has two horizontal ports at 90° angles. The chamber can be rotated in the cube. When the two ports are in front of the windows, measurements can be performed. A rotation of 180° will protect the beryllium windows during treatments at $p < 5$ bar and $T < 750$ K. The sample holder is installed on flange (C) on top of the spherical reaction chamber. Electrical and gas feed throughs are mounted on this flange as well.

1.2. The Energy Range 250–1000 eV

In the energy range of 250–1000 eV, special efforts have to be dedicated to handle the absorption of the gas phase. This problem is obvious in studies at absorption edges of elements present in the catalyst and in the gas phase as well.

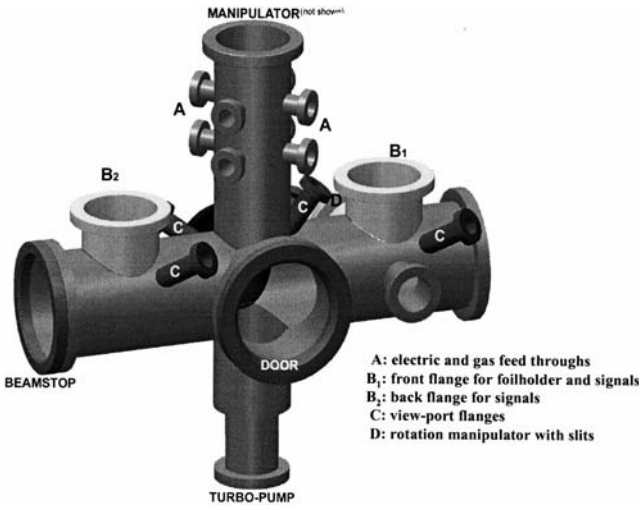

Figure 2. Schematic drawing of the vacuum chamber. The length of the chamber is 90 cm.

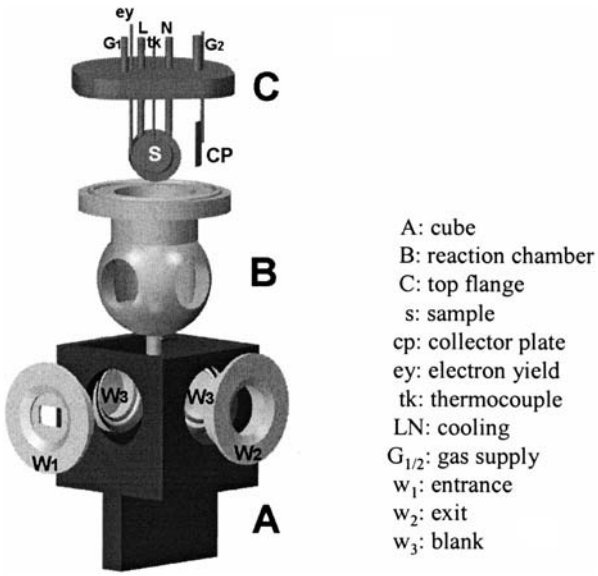

Figure 3. Schematic drawing of the *in-situ* cell assembly for measurement in the energy range 1<hν<3.5 keV. A: a stainless steel cube with window holders; B: the reaction chamber; C: the flange containing the sample holder and all feed throughs.

The *in-situ* cell working in the range of 250–1000 eV, which is present here, is based on the total electron yield detection mode. A core hole is created by absorption of a photon of corresponding energy. This core hole recombines with an electron of a higher shell. The recombination might be radiant. In this case, a photon will be emitted. The detection of these photons is named fluorescence yield. However, the recombination might be non-radiant as well. The energy that is released by the recombination is used for the emission of an Auger electron. This Auger electron creates secondary electrons within the catalyst and within the gas phase. The detection of these electrons is called total electron yield mode.

Total electron yield (TEY) detection has long been used only for XAS studies of surface adsorbates under clean ultra high vacuum conditions [2]. The surface sensitivity strongly depends on the absorption edge energy since it is determined by the escape length of the Auger electron [3]. Its variation extends from a few tens of Ångstroms at sub-keV absorption edges to several thousand Ångstroms for X-ray energies above 10 keV. TEY-XAS data under reaction conditions have so far been obtained mainly for elements with atomic number Z above 15 ($E_b \geq 2000$ eV). This is due to the insufficient transmission of X-ray window materials and due to strong absorption of the soft X-ray photons passing through the gas phase before reaching the sample (see Fig. 1). Knop-Gericke et al. presented a XAS detector system that is suitable for *in-situ* XAS investigations in the soft energy range 250 eV $\leq$ hν $\leq$ 1000 eV under gas/solid reaction conditions [4]. The experimental correlation of the electronic structure of the active surface phase, during the surface reaction with the simultaneously monitored reaction rate and monitored in the gas phase, is a strong advantage of the present design. The soft X-ray absorption energy range is of significance for heterogeneous catalysed reactions of organic molecules by solid surfaces of, for example, noble metals. The K-absorption edges of the low Z-elements carbon, nitrogen and oxygen, which are the constituent elements of organic molecules, are located between 280 and 550 eV. In addition, the L-absorption edges of the 3d-transition metals are also available in this energy range. The TEY technique has advantages over transmission detection as most single crystals and thin film substrates are too thick to be penetrated by low energy X-ray beams. The TEY mode also exhibits advantages over the fluorescence mode, since experimental artifacts are absent [5], [6], and for low Z-elements, the (non radiant) electron yield is close to 1 [2]. Additionally, the surface sensitivity of the TEY detection is high because of the low escape length of the KLL and LMM Auger electrons of only a few tens of Ångstroms. The TEY detection also avoids the self-absorption problems that complicate fluorescence measurements of concentrated samples [7, 8].

It is necessary to collect the XAS of the gas phase during the gas/solid reaction in order to monitor the reaction rate, as the activity of catalysts will depend critically on the conditions of the actual experiment. The set-up used to measure the XAS does not permit a transformation of kinetic results obtained in an ideal reactor system. Therefore, conversion must always be measured during the XAS experiment. Reliable insights into the structure-activity relationship result from a correlation of the surface electronic and geometric structure with the rate of reaction.

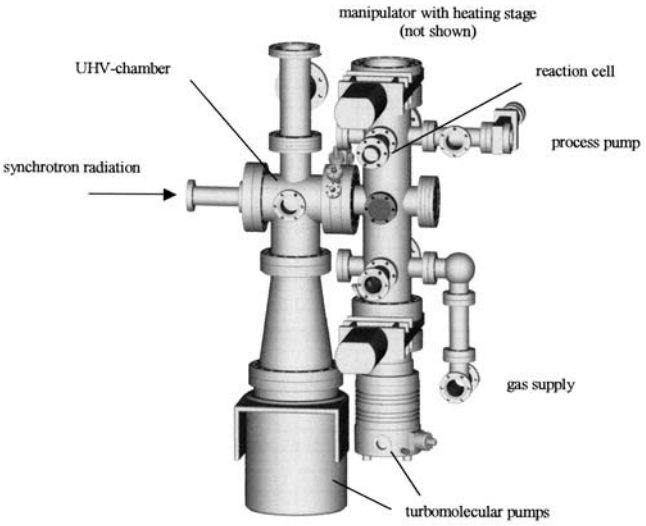

Figure 4. Cross section drawing of the *in-situ* XAS set up built for measurements in the energy range $0.25 < h\nu < 1.0$ keV. The vacuum chamber is shown on the left side, connected by a double flange to the reaction cell.

In Fig. 4, a drawing of the setup is shown. The chamber consists of a reactor and an UHV-pumping stage, which are made of stainless steel and are connected by a double flange. The left part of the chamber (UHV-pumping stage) is connected to the beamline of a synchrotron radiation facility. This part can be evacuated down to 10^{-9} mbar. It is equipped by a gold-covered Cu-grid to monitor the photon flux provided by the beamline. The UHV pumping stage is further equipped with a shutter to shield the X-ray window from the white light of the monochromator. The X-ray photons pass the X-ray window and reach the right part of the chamber that is the reaction cell. The X-ray window material can be fitted to the system under investigation. The analysis of the data will be more reliable when a material is used that does not show absorption features in the relevant energy range. Polyimide, Al and SiN_x have been used successfully in different heterogeneous catalytic reactions. A foil of these materials is glued on a CF16 flange that has a 2 mm hole in the middle. The windows were constructed for pressure differences in the range of 100–1000 mbar, depending on the diameter, thickness and mechanical support of the window. A tube of 100 mm diameter forms the reaction cell (Fig. 5). It can be evacuated to a pressure of 10^{-8} mbar. Mass flow controllers are adapted to the reaction cell, which allow defined gas fluxes to the reaction cell. The gate valve between the turbo molecular pump and the reaction cell will be closed during measurements under dynamical gas feed. The reaction cell volume is either pumped by a process pump or can be used in the batch mode as well. The pressure in the reaction cell can be selected in the range of 10^{-4}–10 mbar.

The catalyst is mounted on a *xyz*-θ-manipulator in the center of the reaction cell and it can be moved in *x* and *y* directions by $\pm$12 mm. The sample can be removed from the reaction cell in *z* direction. The manipulator and the reaction cell volume can be separated by a gate valve to change the sample after venting the manipulator volume. The catalyst itself is mounted on a resistance heater. The heater consists of a boron

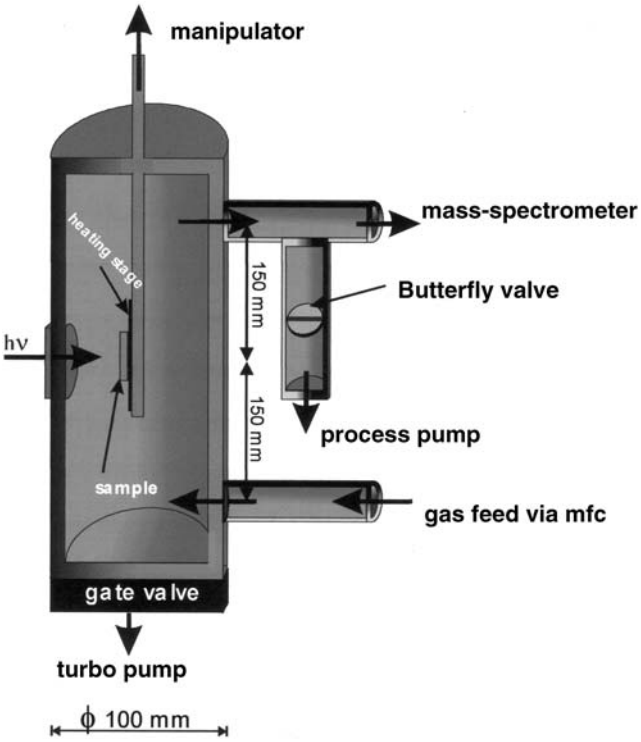

Figure 5. Cross section drawing of the reaction cell. The gas feed is provided by mass flow controllers. The gases flow from down over the catalyst, pumped by an adjustable process pump. The outlet gas is analyzed using a mass spectrometer. The sample stage with the heating and the X-ray window are included in the drawing as well. The detector system, which is located between the X-ray window and the sample, is not shown for reasons of clarity.

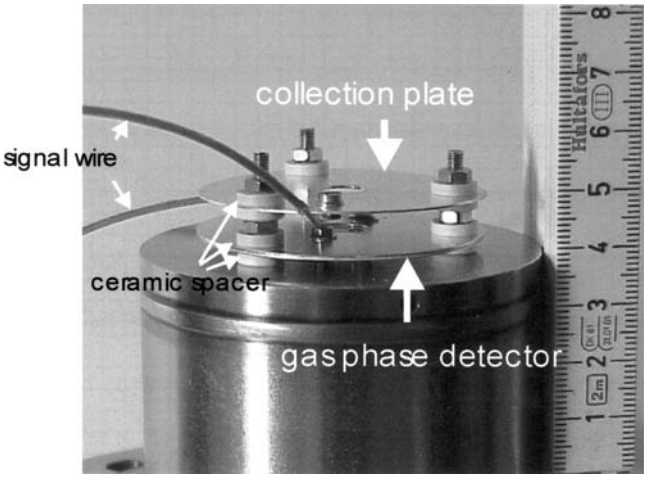

Figure 6. Photograph of the detector system. The two detector plates for gas phase and sample electron signals are visible. The signal-wires of the plates are shown as well. The detector system is mounted on the double flange connecting the vacuum chamber with the reaction cell.

nitride-covered graphite layer, which can be heated by electrical current up to 1300 K. The temperature is measured by a chromel-alumel thermocouple.

The reaction cell contains a detector system for the recording of X-ray absorption spectra in the total electron yield mode. Fig. 6 shows a photograph of the detector system. A schematic drawing of the detector system, including the X-ray window and the sample, is shown in Fig. 7. It consists of two 50 mm diameter Al plates with a hole of 8 and 10 mm in the collection plate and the gas phase detector, respectively. The synchrotron radiation passes the X-ray window and the two holes before impinging on the sample. A positive voltage of 4.5 . . . 27 V is applied to the collection plate using a battery box. The gas phase detector with the Au covered Cu grid is grounded. The signals from both detectors are amplified and then monitored by computer. The sample itself is connected via a signal wire to an additional current amplifier. This signal contains information of the absorption coefficient as well, since the electrons emitted after the absorption process leave holes, filled by electrons via the signal wire. This drain current is measured. The gas composition in the reaction cell is measured by a differentially pumped mass spectrometer (Fig. 5).

The gas atmosphere in the reaction cell acts as an amplifier for the electrons, since the Auger electrons emitted from the catalyst surface create new electrons through the ionization of gas phase molecules. The amplification factor depends on the used gas species and on the pressure [13]. Fig. 8 shows the calculated total electron yield (TEY, light bars) signal as a function of the oxygen pressure and the kinetic energy of the primary electrons (Auger electrons and secondary electrons leaving the solid). The number of detected electrons is plotted, normalized to the number of primary electrons. The dark bars are experimental values of a Cu L_3-edge measurement. The different amplification and the relevant multiplication factors for different energies are obvious.

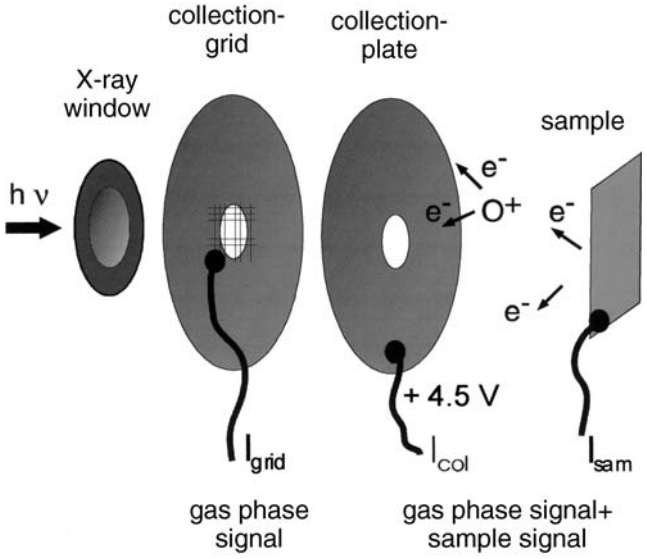

Figure 7. Schematic drawing of the detector system. Within the drawing plane, the synchrotron radiation passes the X-ray window from left to right, which is located between the vacuum chamber and the reaction cell. In the reaction cell, the detector system is mounted. It provides three TEY signals (I_{grid}, I_{col}, I_{sam}). Auger electrons created by the absorption process will be multiplied by the interaction with the reaction gas and will be detected by the collection plate, which is provided with a positive electrical potential.

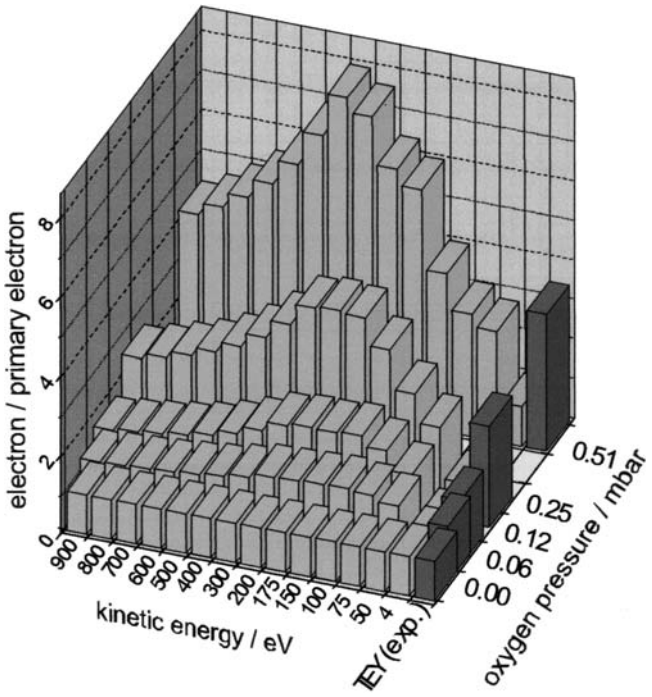

Figure 8. TEY signal as a function of the oxygen pressure and the kinetic energy of the primary electrons.

Although this method represents a contribution to overcome the pressure gap, *in-situ* XAS in the energy range below 1000 eV can be applied only for pressures in the mbar range. Real catalytic reactions will be performed at much higher pressure of at least one bar. For example, the reaction profile of the methanol oxidation on copper detected in the *in-situ* cell is identical with the profile observed in a tube reactor operated at 1 bar. Fig. 9 compares the specific activities of different vanadium phosphorus oxide catalysts in the n-butane oxidation to maleic anhydride (MA). However, the catalytic activity observed at 1 bar correlates to the catalytic activity observed in the *in-situ* soft XAS cell at 2 mbar, just as a catalyst with high specific activity at 1 bar is active at 2 mbar as well. A low catalytic activity at 1 bar addicted a low activity at 2 mbar. The relative activities at one bar are similar to the activities observed at 2 mbar in the *in-situ* cell. These comparisons show that the results obtained with the *in-situ* cell can be transferred to real catalytic conditions.

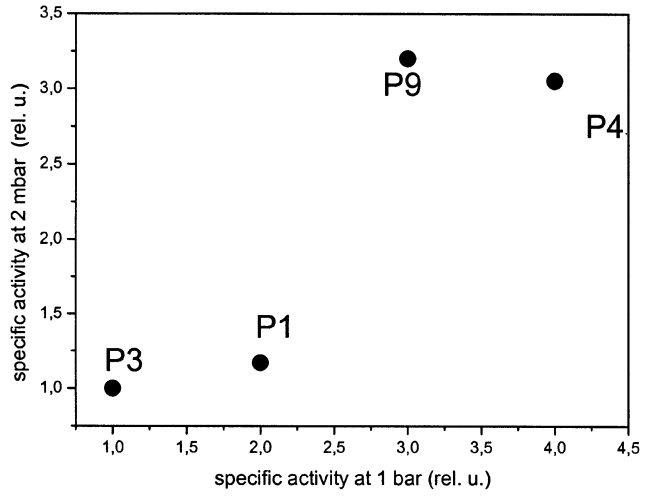

Figure 9. Correlation between specific catalytic activity in the n-butane oxidation to maleic anhydride (MA) determined at 1 bar and at 2 mbar in the *in-situ* cell.

2. SPECTRAL SHAPE ANALYSIS

The soft X-ray absorption spectral shape is given by exactly the same formula as for hard X-rays. The X-ray absorption intensity is given as a squared matrix element (M^2) times the density of empty states (ρ), i.e.,:

$$I_{XAS} \sim M^2 r \tag{1}$$

In case of the carbon, nitrogen and oxygen K edges, calculations exactly as described in the chapter on XANES can be applied [2]. In the case of systems with metal edges with soft X-rays, things are different. The 2p edges of the 3d-metals are most often studied. These edges are affected by multiplet effects that break the direct analogy between X-ray absorption spectral shape and density-of-states.

2.1. Multiplet Effects

Equation 1 does not hold if the overlap of the core wave function and the valence wave functions are large. In the case of 3d-systems, the 1s core state does not (notably) overlap, in contrast to the 2s, 2p, 3s and 3p core wave functions. The 2s and 3s core states cause only an exchange splitting, but the overlap of the 2p and 3p core states causes a complex spectral shape. The 2p X-ray absorption edges are often used for 3d-transition metals and have energies between 400 and 900 eV. A successful analysis method has been developed based on a charge transfer multiplet model.

Faced with the situation of a solid catalyst with its extended valence states and a localized core hole, the point of the matter is to find the best way to treat the X-ray absorption process. The multiplet model starts with a completely localized approach. Only the 3d-states are maintained for the valence band and the transition of the 2p core state to the 3d valence state is calculated, including the coupling of the 2p with the 3d electrons. It is noted that these interactions are not treated correctly by (normal) Local-Spin-Density based calculations. The solid state effects are included in two stages. First, the local symmetry is included within crystal field theory. For example, in octahedral symmetry, this implies that the 3d-states are split into their t_{2g} and e_g constituents. The second ingredient is the inclusion of charge transfer: the inclusion of a second configuration for which an electron has jumped from the valence band to the 3d-band. The overall ground state is a linear combination of $3d^N$ plus $3d^{N+1}L$, where L is a hole in the ligand band. The same approach is used for the final states and the X-ray absorption transition is calculated. This so-called charge transfer multiplet model gives adequate descriptions of the 2p X-ray absorption spectra of transition metal ions in solids [9–11].

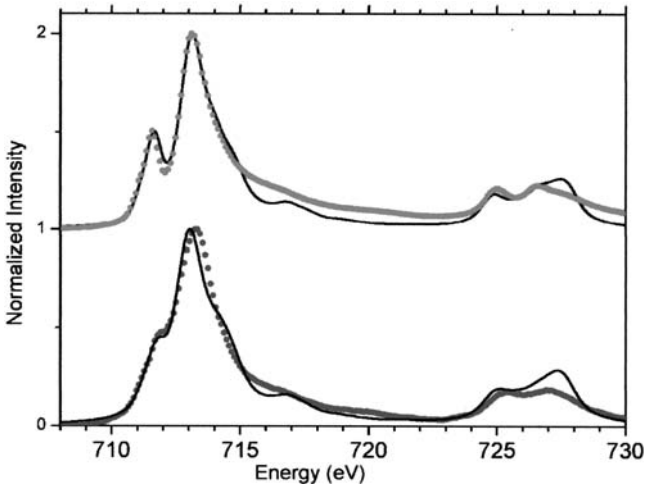

Figure 10. Charge transfer multiplet simulations (solid lines) compared with the experimental spectra (points) of Fe_2O_3 (top) and the oxidized Fe/ZSM5 (bottom).

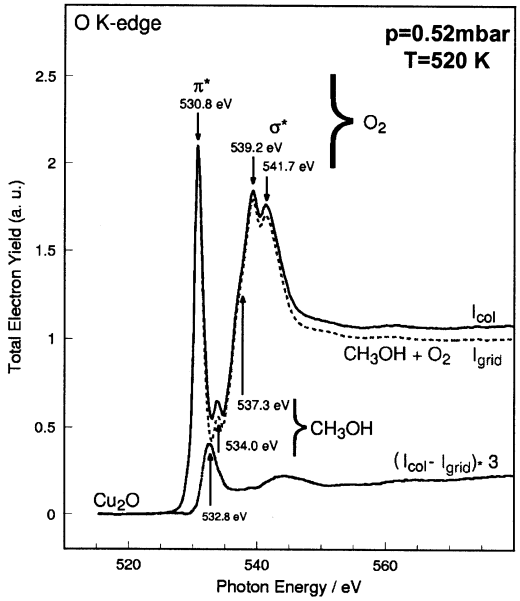

Figure 11. Example for data analysis of XANES spectra measured at an absorption edge of an element that is present in the catalyst and in the reaction gases. A polycrystalline copper foil was heated up to 520 K in a mixture of methanol and oxygen at 0.52 mbar. The plotted spectra were normalized to the photon flux to the same intensity at the π* resonance of molecular oxygen. A linear background was subtracted. The characteristic absorption feature of the gas phase components dominates both the collection plate signal (I_{col}) and the gas phase detector signal (I_{grid}). The absorption spectrum of the catalyst surface is obtained by the subtraction of both spectra from each other. The O K edge absorption spectrum of Cu_2O is revealed under the special conditions.

As an example, we discuss the 2p X-ray absorption spectrum of over-exchanged Fe/ZSM5 under oxygen atmosphere at room temperature compared to Fe_2O_3 as shown in Fig. 10. The Fe $L_{2,3}$ X-ray absorption spectral shape ranges from approximately 700 to 730 eV. Fig. 10 shows the comparison of the iron 2p spectra of the oxidized Fe/ZSM5 sample (bottom) with Fe_2O_3 (top). The iron 2p spectrum of Fe_2O_3 corresponds well to the theoretical curve (solid line) that has been calculated using the two configurations $3d^5$ and $3d^6L$ for the ground state. The oxidized Fe/ZSM5 sample can be explained from the same configurations, however, with a reduced crystal field splitting. The overall crystal field splitting is1.4 eV for Fe_2O_3 and 1.0 eV for the oxidized Fe/ZSM5 sample. The analysis shows that the oxidized Fe/ZSM5 is completely oxidized to a trivalent state within an octahedral surrounding. The fact that the crystal field splitting of Fe/ZSM5 is considerably smaller than that for Fe_2O_3 suggests (on average) less bonding between iron and its six oxygen neighbors. In section 3.5., we discuss the oxidation-reduction behavior of Fe/ZSM5 by making use of the *in-situ* detected 2p X-ray absorption spectra [12].

2.2. Data Treatment of Electron-Yield Signals

In many reactions, the contribution of the gas phase dominates the detected spectra. In this chapter, the manner in which to treat the data to extract the absorption spectra of the catalyst will be described.

Four signals related to the X-ray absorption process are collected simultaneously in every scan (Fig. 7). These are the signals of the grid in the UHV-pumping stage that can be used for normalization, the sample current and the signals of the collection plate, and the gas phase detector. The number of photons that reaches the sample does not depend only on the photon flux of the used beamline of the synchrotron radiation facility, but also the X-ray window. A spectrum detected under vacuum conditions is used for the normalization with respect to the absorption of the X-ray window. The gas phase detector signal (I_{grid}) consists of Auger electrons and secondary electrons created by the X-ray absorption process in the gas phase molecules. This signal is needed to extract the absorption signal of the catalyst at adsorption edges of elements that are present in the gas atmosphere as well. Absorption spectra recorded at the carbon, nitrogen and oxygen K edges are very often the focus of interest in X-ray absorption spectroscopy investigations of heterogeneous catalytic systems. The electrons detected by the collection plate are created by the absorption process in the solid state of the catalyst and in the gas phase. This accounts for the sample current (I_{sam}) as well, since the surface of the catalysts acts as a collection plate. A signal, which is exclusively due to the absorption of the catalyst, can be extracted from the collection plate signal, despite the huge influence of the gas phase. This is achieved by the subtraction of the gas phase signal (I_{grid}) from the collection plate signal that was detected simultaneously. The procedure is demonstrated in Fig. 11 for the O K edge spectrum of a copper foil acting as a catalyst in the selective oxidation of methanol to formaldehyde. The raw data are normalized, first by a suitable reference spectrum, an untreated sample measured in vacuum or in a gas, which does not show absorption features in the relevant energy range. This is necessary, since the photon flux is not constant as a function of the photon energy due to the contamination of optical element within the beamline. The data analysis will be continued by the subtraction of the pre-edge intensity followed by the normalization of both spectra to the same inten-

sity at an energy at which only a contribution of the gas phase to the signal is expected. In the example shown in Fig. 11, it is the π*-resonance of molecular oxygen in the gas phase. The authors assume that no molecular oxygen is present on the polycrystalline Cu surface at 520 K. The extraction of the surface sensitive catalyst signal is finished if no negative intensities appear in the spectrum. It is obvious that the contribution of the catalyst signal in the collection plate signal is lower than 10%. The collection plate signal is dominated by the π*-resonance of molecular oxygen at 530.8 eV. The σ*-resonance of molecular oxygen at 539.2 eV and 541.7 eV, and Rydberg transitions of methanol at 534.0 eV and 537.2 eV, are detected as well. These structures can be used for energy calibration. The extracted spectrum shown in Fig. 11 corresponds to O K edge absorption spectrum of copper(I) oxide (Cu_2O), which can be concluded by comparison with literature data [14]. In other reaction, typical gas phase contributions can be used to do the gas phase substraction. In the case of ammonia oxidation over copper, the sharp N-H* resonance of the gas phase signal is used for the indication of a proper gas phase subtraction [15]. In general, the difference spectrum should not show negative intensities.

3. EXAMPLES OF SOFT X-RAY ABSORPTION ON CATALYTIC SAMPLES

3.1. Structural Properties of Mg-Al Hydrotalcite Solid Base Catalyst

In a recent paper, van Bokhoven et al. investigated the flexibility of (Mg-Al) hydrotacite (HT) structures by *in-situ* XAFS spectroscopy at the Mg and Al K edges [16]. This study gives further proof of the necessity to apply *in-situ* methods for the investigation of catalysts, because the spectra measured ex situ differ significantly from the spectra detected *in-situ*. Hydrotalcite ($[Mg_6Al_2(OH)_{16}](CO_3)\cdot 4H_2O$) is a layered double hydroxide that is related to brucite $Mg(OH)_2$ in which the Mg cations occupy the centers of hydroxyl octahedra. These octahedra are joined along their edges, forming a layered structure composed of hexagonal platelets [17]. In hydrotalcite, some of the Mg^{2+} ions are replaced by Al^{3+} ions, inducing a net positive charge in the cation layers. Charge-balancing anions (usually CO_3^{2-}) and water molecules are present in the interlayers. It is well documented that for hydrotalcites, physisorbed and interstitial water is removed at temperatures above approximately 325 K and 460 K, respectively. At higher temperatures, the hydrotalcite undergoes dehydroxylation and decarbonylation, producing H_2O and CO_2. A modified hydrotalcite has been proven to be active in the coupling of various ketones and aldehydes in base-catalyzed aldol condensation reactions, which is an industrially used reaction for the production of vitamin A. The application of solid base catalysts, instead of currently used homogeneous alkaline bases, allows the recycling of the catalyst reducing the chemical waste. Hydrotalcites show high activity in catalytic reactions already at low temperature. These properties offer interesting possibilities for the commercial use of hydrotalcite.

The authors measured the Mg and Al K edge of HT spectra at room temperature after heat treatments at different temperature and compared those to measurements that were taken at high temperature. The Mg K edge X-ray absorption spectrum of the as-synthesized hydrotalcite (HTa.s.) shows octahedral coordinated Mg centers according to Fig. 12. HTex'T' assigns the hydrotalcite calcined ex situ at maximum temperature T. The hydrotalcite shows a change in the spectrum after heating above 475 K, indicating a change of the octahedral coordination. The spectrum of HTex725 resembles the spectrum of MgO, but it shows less fine structure. After rehydrating the sample at room temperature, the spectrum is identical to the spectrum of the starting material HTa.s. The Al K edge spectra indicate a change after heating the sample at 475 K as shown in Fig. 13. The changes show a decrease in intensity at 1572 eV and an increase of the resonance at 1566 eV, indicat-

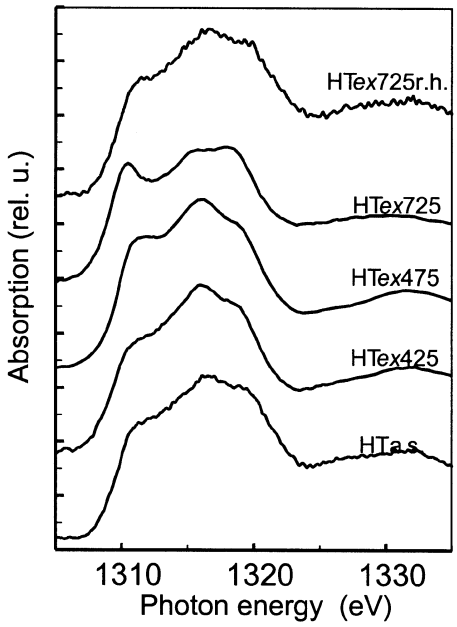

Figure 12. Mg K edges of heat-treated hydrotalcite, showing a gradual change in the spectra after treatment above 475 K. A restoration of the structure is visible for a rehydrated sample that had previously been heated to 725 K.

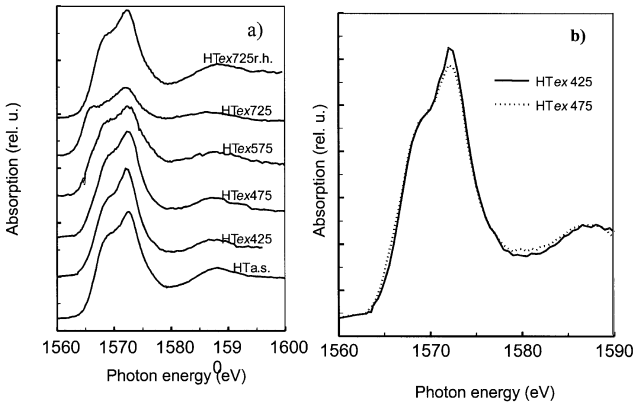

Figure 13. a) Al K edges of ex situ heat-treated hydrotalcite, showing a gradual change in the spectra of samples treated at temperatures above 475 K; b) Al K edge of HT*ex*425 and HT*ex*475, showing a change in aluminum coordination.

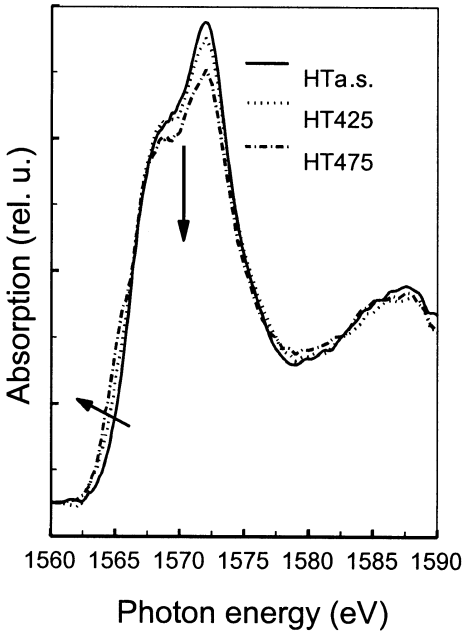

Figure 14. *In-situ* measured Al K edge spectra of hydrotalcite showing the appearance of lower coordinated Al sites already at 425 K.

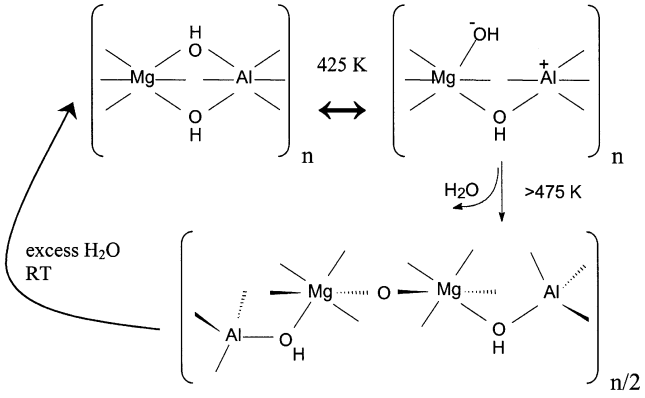

Figure 15. Processes occurring during heat treatment of hydrotalcite. At temperatures below 425 K, a reversible change in aluminium coordination occurs. At temperatures higher than 475 K, the magnesium coordination alters, making the changes irreversible upon cooling. Adding an access of water restores the original structure.

ing a decrease of octahedral Al, while tetrahedral Al centers appear. This change in spectrum is observed at higher temperatures as well. Rehydration at RT (HT*ex*725r.h.) reverses the Al coordination of the heated HT to the original octahedral coordination. The Mg K edge spectra of HT425 are the same as the spectrum of HTa.s. (HT'T': 'T' indicates the temperature at which the sample was measured.) Fig. 14 shows the Al K edge spectrum HT425 differing from the spectrum HTa.s. This is a deviation from the results the authors revealed from ex situ calcination. The intensity at 1568 eV and 1572 eV is decreased and the energy of the edge is shifted toward lower energy. This is due to an increase of the tetragonal Al content. The authors conclude this by comparing the spectra to X-ray absorption spectra of reference samples. These results were accompanied by EXAFS data of the same samples. An acceptable fit of the Fourier transformed Al K edge EXAFS spectrum of HTa.s. was achieved by using one shell of octahedral coordinated oxygen neighbors. The quality of the fit could not be statistically improved by adding an additional shell. A good quality fit for the spectrum of the sample HT*ex*725 was obtained after addition of an extra shell: one shell at 1.86 A for the octahedral coordinated oxygen and the second shell at 1.56 Å for the tetrahedrally coordinated oxygen.

Obviously, the change in coordination observed after calcination at 425 K is fully reversed upon cooling down the sample to room temperature. However, the changes in the Al coordination are irreversible as soon as the Mg coordination is altered, which is observed at 475 K.

The authors suggest a working hypothesis given by the scheme of processes occurring during the calcination of HT as proposed in Fig. 15. The coordination of Al is lowered at 425 K by breaking of Al-OH bonds. At this temperature, no dehydroxylation occurs at the cation layer. At 475 K, a proton of a hydroxide could diffuse to an Al-OH group yielding a water molecule. Since the water molecule coordinates less strongly to the aluminum center, the aluminum coordination is lowered. The water molecule will not completely lose contact with the aluminum center because the temperature is too low. Therefore, the structural change is completely reversible after cooling to room temperature. The dehydroxylation process starts at temperatures above 475 K induce changes in the Mg and Al coordination. The process is not reversible as indicated in Fig. 15. The breaking of Mg-OH bonds induces the formation of Mg-O-Mg bonds, which forms the rocksalt MgO-like phase. The evolution of water from the sample will conduct the breaking of Mg-OH bonds. Once the rocksalt phase is formed, changes in structure are not reversible after cooling the sample. Rehydration at room temperature fully reverses the changes in coordination even after the hydrotalcite has been calcined to 725 K.

This is another example showing that the structure of a catalyst observed under *in-situ* is different from the structure estimated from *ex-situ* measurements due to reverse effects.

3.2. Methanol Oxidation Over Polycrystalline Copper

The methanol oxidation over copper was studied by measuring X-ray absorption spectra at the C and O K edges and at the Cu L edges in oxygen/methanol flows at 1 mbar [18]. The existence of different oxygen species on the copper foil surface that behave differently in the methanol oxidation is shown. The relation between surface species and reaction paths, like partial or total oxidation, was made by correlation between the intensity of the relevant oxygen species and the yield of the corresponding reaction products. The reaction rates and the electronic state of the active catalyst surface are measured simultaneously in an *in-situ* experiment. In Fig. 16, a model is suggested for the active surface of the copper catalyst in the course of methanol oxidation, indicating that different oxygen species are present during the catalytic reaction. The corresponding O K edge XANES spectra are shown in Fig. 17. Two types of oxygen species can be distinguished

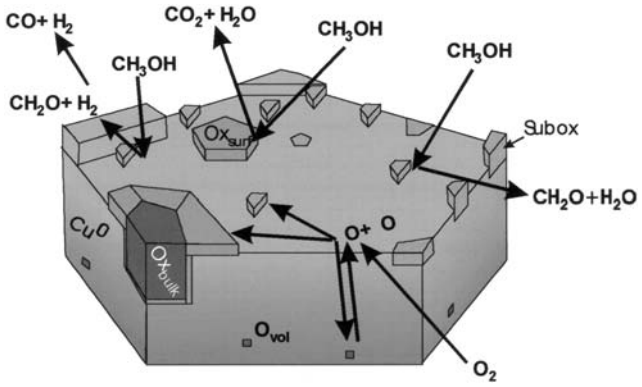

Figure 16. Active surface of the copper catalyst showing different coexisting oxygen species. The arrows indicate the interaction of the gas phase with the copper surface. The bulk oxide Cu_2O and the thin surface oxide Ox_{surf} are visible. Both convert methanol to CO_2 and water. The atomic weakly bounded species located on the surface is shown as well. This species correlates with the yield of formaldehyde. The active state of the catalyst is characterized by a metallic surface, whereas oxygen is incorporated in the volume that will be exchanged with oxygen surface species.

according to their catalytic functionality. These are the oxidic species Ox_{surf} (A_1) and Ox_{bulk} (A_2) and, on the other hand, a suboxide (Subox) indicated as B+C. The different resonance energies of A_1 at 531.7 eV due to the surface oxide and of A_2 at 532.8 eV due to copper (I) oxide reflect the influence of the metallic substrate on thin layers of oxide, whereas thicker

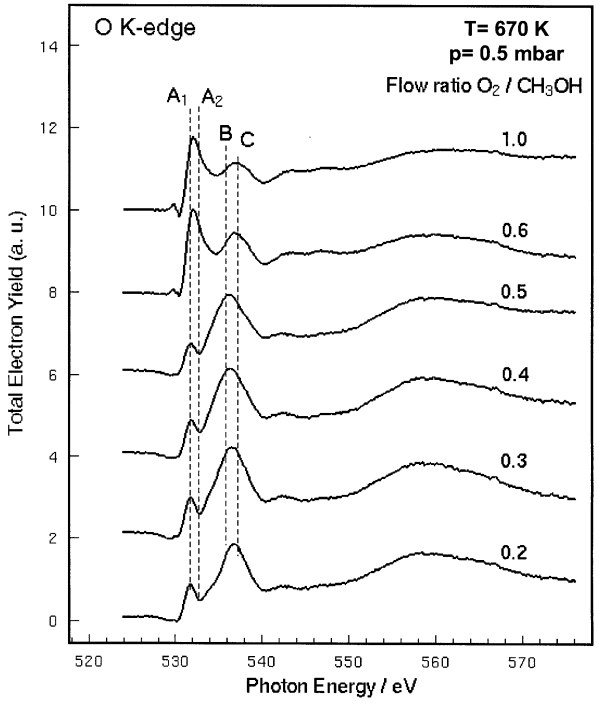

Figure 17. O K XANES of a copper foil at 670 K as a function of O_2/CH_3OH flow ratio. The pressure was 0.5 mbar. The spectra are dominated by the surface oxide (A_1) and the bulk oxide (A_2) for O_2/CH_3OH ratios above 0.6. The spectra change after increase of the abundance of CH_3OH. A suboxide structure (B+C) is dominating for O_2/CH_3OH ratios below 0.5.

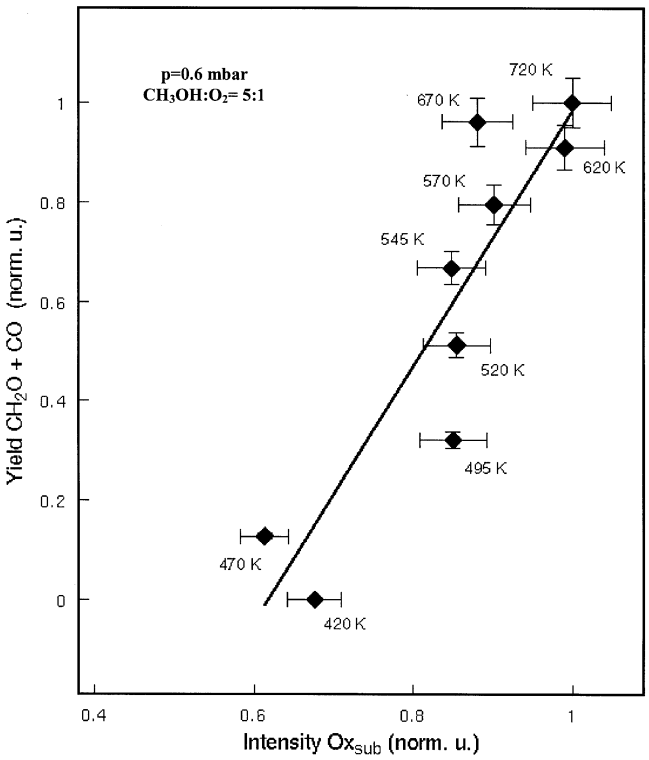

Figure 18. Yield of CH_2O+CO plotted as a function of the amount of suboxide (spectral intensity B+C in Fig. 15). The temperature was varied at an O_2/CH_3OH gas flow ratio of 0.2. The pressure was 0.6 mbar.

layers appear indistinguishable from bulk oxide. Both oxidic features Ox_{surf} and Ox_{bulk} show O1s →O2pCu3d electron transition, whereas the new suboxide B+C is characterized by the O2pCu4sp hybridization. The integrated intensity of the resonance B+C is plotted in Fig. 18 for an O_2/CH_3OH gas flow ratio of 0.2 at 0.6 mbar as a function of temperature. The linear correlation indicates that the suboxide catalyses the partial oxidation of methanol to formaldehyde (Fig. 18). The abundance of Ox_{surf} and Ox_{bulk} on the surface correlates negatively with carbon dioxide and water (not shown), which are the products of the total oxidation of methanol. Copper(I)oxide is formed from Ox_{surf} that is present on the surface as a thin film by increasing oxygen coverage. Therefore, Ox_{surf} represents a first step of the bulk oxide formation. Two properties of the catalyst surface are crucial for partial oxidation of methanol to formaldehyde. The surface has to exhibit metallic centers (Cu^0). An increasing coverage of the surface by oxidic species inhibits the reaction. The surface of the catalyst is covered by copper(I)oxide below a critical temperature depending on the methanol/oxygen ratio. This state is not active in the partial oxidation. On the other hand, the yield of formaldehyde correlates with the spectral intensity of an atomic covalently bonded oxygen species (Subox) as plotted in Fig. 18. This suboxide features a completely different electronic structure compared to the known copper(I) and copper(II)oxide. Cu_2O and CuO are characterized by the hybridization of O2p and Cu3d molecule orbitals, whereas the Subox is formed by O2pCu4sp interaction. Since the suboxide is present in different environments, a distribu-

tion of its resonance energies is observed. For this reason, the spectral feature of the Subox shows larger FWHM compared to Ox_{bulk} and Ox_{surf}. The authors assume that the formation of Subox is governed by the incorporation of oxygen in the catalyst, which might create strong rearrangement of the surface forming defects upon the reaction [4, 19]. The species Subox is metastable. Therefore, it can be detected only under reaction conditions. It decomposes within copper metal and copper(I)oxide under different environments [4]. Unfortunately, the structure of this atomic oxygen species cannot be made accessible and even the definite function of Subox is not clarified yet. The authors speculate that Subox acts as a marker indicating the actual active center of partial oxidation. A direct intervention of Subox in the catalytic reaction cannot be excluded.

The reaction temperature profile of this reaction, measured at 0.5 mbar in the *in-situ* reaction cell, is identical with the profile measured over a copper tube at 1 bar. The catalyst was an empty copper capillary wound into a spiral of a path length of 100 cm. Therefore, the results obtained in this *in-situ* XANES study can be transferred to real catalytic conditions [18]. This study demonstrates the importance of *in-situ* study, because the new oxygen species Subox that is responsible for methanol oxidation can be detected only under reaction conditions. At room temperature, copper oxide is formed by oxygen solved in the bulk, and therefore, no suboxide can be observed *ex-situ*.

3.3. Ammonia Oxidation Over Polycrystalline Copper

Mayer et al. investigated the ammonia oxidation over copper using *in-situ* XAS in the soft energy range. Two reaction paths are known for this reaction. The total oxidation of ammonia is given by

$$4NH_3 + (3 + 2x)\,O_2 \rightarrow 4\,NO_x + 6\,H_2O\ (x = 1, 2) \quad (2)$$

and the partial oxidation of ammonia is described by

$$4NH_3 + 3O_2 \rightarrow 2N_2 + 6\,H_2O \quad (3)$$

Polycrystalline copper foil was used as a model catalyst in this investigation. This foil was prepared to get different initial states of the catalyst like CuO, Cu_2O and metallic copper. In a gas flow of NH_3/O_2 = 1:12 at 0.4 mbar using CuO as initial state, a reaction at temperatures above 575 K was observed. A deactivation of the catalyst started a few minutes after the temperature was increased, shown by the mass spectrometry spectra presented in Fig. 19. The simultaneously measured N K edge and Cu L_3 edge XANES spectra are plotted in Fig. 20A. The resonances observed in the Cu L_3 edge shown in Fig. 20B at 465.6 eV and 466.7 eV are due to CuO and Cu_2O, respectively. The resonance at 467.1 eV, which appears after 70 min. at 670 K can be assigned to copper(I)-nitride. Running the reaction at 675 K for one hour induced the formation of copper nitride that inhibited the catalytic reaction. An oxidation of the copper nitride to copper oxide is not observed under the reaction conditions. Even the decrease of the NH_3/O_2 ratio up to 1:50 does not prevent the formation of copper nitride. Using CuO as the initial state, the authors observed a reaction to mainly NO at 1.2 mbar. During two

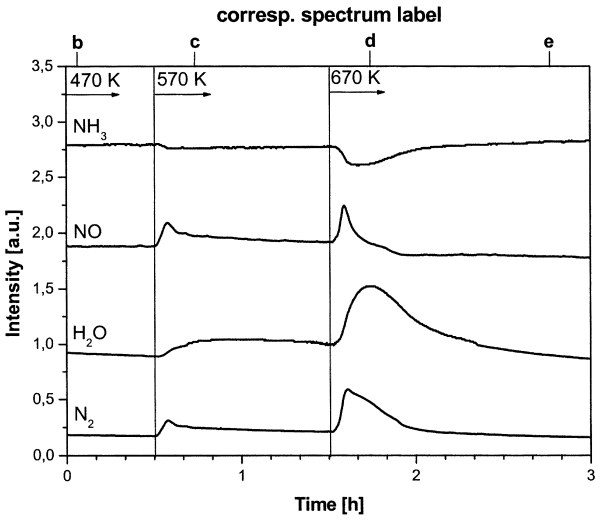

Figure 19. Mass spectrometry spectra of NH_3, NO, H_2O and N_2 of the ammonia oxidation on copper at p = 0.4 mbar, NH_3:O_2 = 1:12, with increasing temperature.

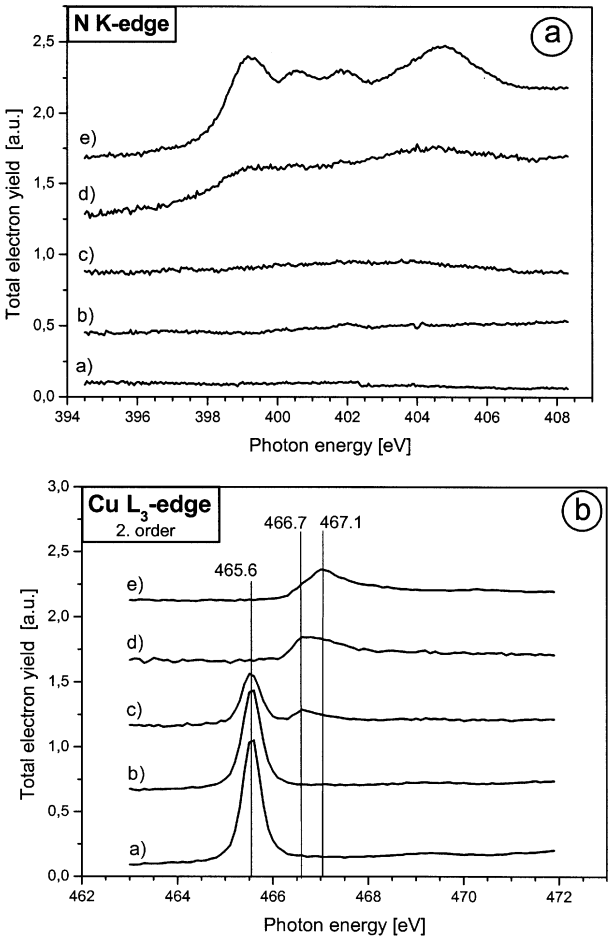

Figure 20. XANES spectra at the N K edge (A) and the Cu L_3-edge (B) during the ammonia oxidation on copper at p = 0.4 mbar, NH_3:O_2 = 1:12 at (a) room temperature, (b) 470 K, (c) 570 K, (d) 15 min. at 670 K, and (e) 70 min. at 670 K (From [15]).

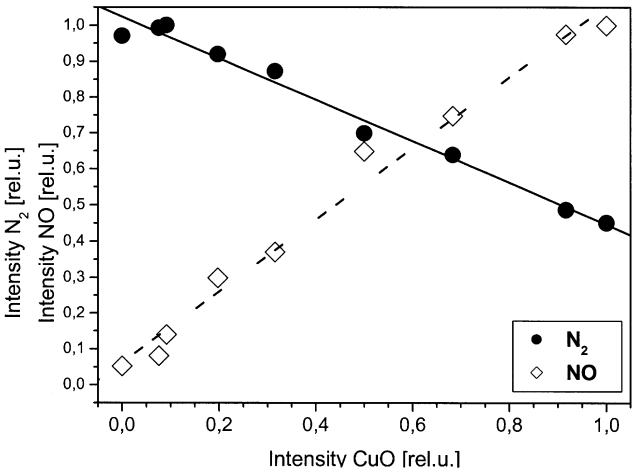

Figure 21. Correlation of the relative intensities of N_2 (—) and NO(– – –) with the intensity of CuO for the ammonia oxidation at 0.8 mbar, 670 K and NH_3:O_2 = 12 (From [15]).

hours at 675 K, the selectivity changed slightly to N_2 and the copper(II)oxide was reduced partly to copper(I)oxide. Using Cu_2O as the initial state, little formation of NO was observed and the selectivity to N_2 was very high. A presence of metallic copper can be excluded, since metallic copper showed activity only after oxidation to copper(I)oxide. Fig. 21 shows the correlation between the yield of NO and N_2 and the spectral intensity of CuO, observed at p = 0.8 mbar. This demonstrates that copper(II)oxide catalyses the total oxidation to NO, whereas the partial oxidation can be achieved only when copper(I)oxide is present on the surface. Therefore, it is suggested that Cu(I)O oxygen is involved directly in the reaction. In this study, no hints were revealed for the co-operation of other oxygen species in the ammonia oxidation. A comparison of the amount of oxygen atoms in the initial state (CuO) of the catalyst and the amount of oxygen atoms that was converted by the reaction clearly proved the catalytic character of the reaction. A deactivation of the catalyst induced by the formation of copper nitride was observed at 1.2 mbar as soon as copper(I)oxide was present on the surface. A direct nitridation of copper(II)oxide was not observed. A comparison of the nitridation at 0.4 and 1.2 mbar shows the influence of the ammonia partial pressure on the Cu_3N formation. The authors suggested the following reaction mechanism for the formation of N_2 and Cu_3N on a Cu_2O catalyst (Fig. 22). The abstraction of hydrogen induces the formation of amide ($NH_{2,ad}$). Two neighboring amide groups form the dimer hydrazine, which decomposes into N_2 and OH [20]. At low partial pressure of ammonia, the formation of hydrazine is disabled, because less neighbored amide groups are present. Therefore, a successive hydrogen separation occurs [21]. The deactivation of the catalyst at 1.2 mbar is slower compared to a pressure of 0.4 mbar, since the probability of the adsorption of two ammonia molecules on neighboring sites is higher at higher pressure. Therefore, the dimerisation and the subsequent decomposition to nitrogen is observed more frequently for higher pressure than the formation of adsorbed nitrogen.

3.4. Epoxidation Over Silver

The well-known activity of silver as catalyst for the selective oxidation of a number of hydrocarbons has generated a large number of investigations devoted to the interaction of oxygen with silver surfaces during the last thirty years. Post-reaction analysis of the surface composition by various surface sensitive methods allowed a number of authors to identify several oxygen species. A model that postulates that the active sites consist of two oxygen species (nucleophilic and electrophilic) was proposed [22–24]. However, in spite of these considerable efforts, the debate over the mechanisms of the ethylene epoxidation over silver and the nature (molecular or atomic)

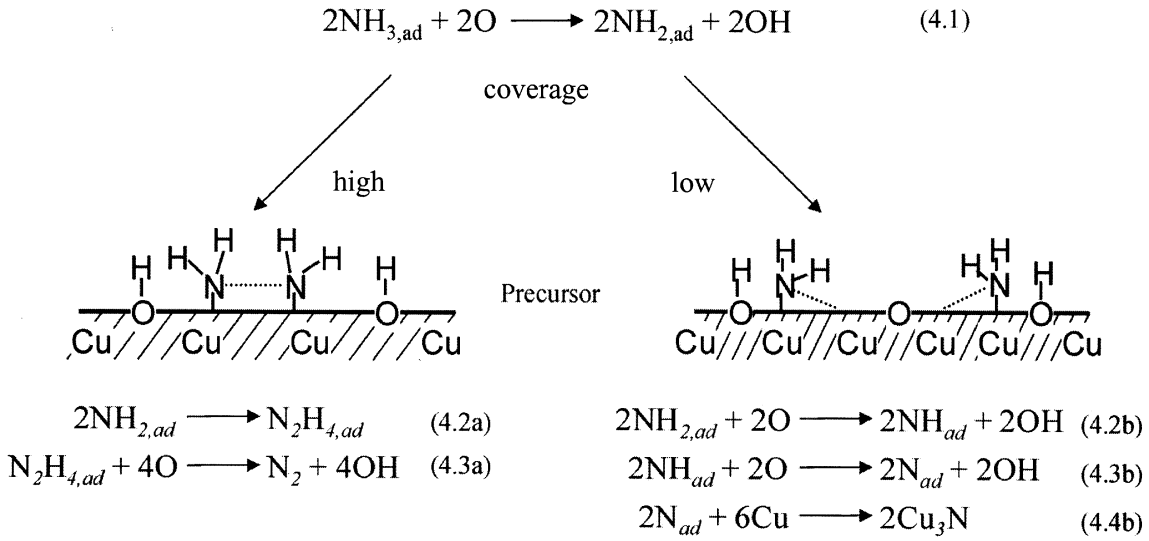

Figure 22. Cu_2O with different coverage of the precursor ammonia, illustrating the reaction steps. High coverage and adsorption on neighbored sites is compared to low coverage and adsorption on abscised sites (From [44]).

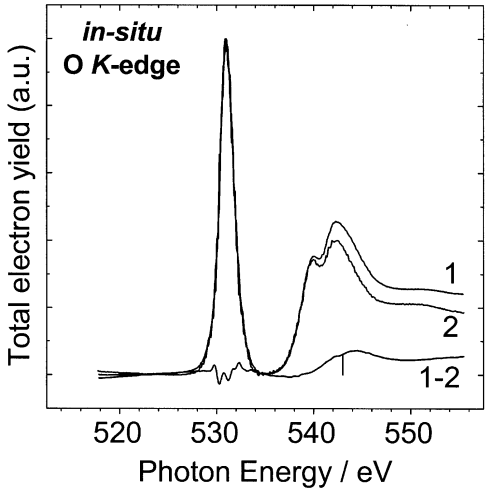

Figure 23. O K edge X-ray absorption spectrum (1) recorded during treatment of a clean polycrystalline silver foil by a C_2H_4 (2%) + O_2 reaction mixture at T = 470 K and p = 2mbar. XAS spectrum of the gas phase (2) and difference spectrum (1–2) are also shown.

of the active oxygen species are kept open by the apparent lack of physical methods to characterize the oxygen overlayers at "high-pressure" conditions where ethylene oxide is obtained amongst the reaction products (pressure>1 mbar). This requires the use of methods that, on one hand, are sensitive to the electronic structure of the oxygen species and, on the other hand, can work in the millibar pressure range. Therefore, *in-situ* XANES spectroscopy was applied for the investigation of the ethylene epoxidation over silver in a study by Bukhtiyarov et al. [25]. *In-situ* O K edge XANES spectra show a broad signal 10–20 eV above the threshold [25]. The comparison of the X-ray absorption spectra with the O 1s and valence band photoemission data allowed the authors to attribute this XAS signal to "electrophilic" oxygen (E_b(O1s)= 530.4 eV), which is suggested to be active in ethylene epoxidation. In Fig. 23, the O K edge absorption spectrum of a polycrystalline silver foil detected under reaction conditions of the ethylene epoxidation at 2 mbar is presented after subtraction of the dominating gas phase contribution (1–2). According to Grant and Lambert, an oxygen pressure of 1 mbar is a sufficient to activate a clean silver foil [23]. The *in-situ* signal from the catalyst is characterized by one broad feature in the photon range of 540–545 eV, as shown in Fig. 23. The energy range of 530–535 eV is featureless within the level of noise. This energy range is characteristic for the absorption into molecular oxygen orbitals. The high noise level induced by the gas phase subtraction might prevent the observation of small signals from adsorbed species. To tackle this problem, the XAS data after evacuation of the reaction mixture were analyzed. A similar feature at ~ 542 eV is observed in the ex situ absorption spectrum after a reaction treatment of 6 h, as shown in Fig. 23. In addition, a small peak around 531 eV is observed. Heating the foil in vacuum up to T = 570 K causes the disappearance of the peak at 531 eV, as shown in Fig. 24, while the signal at 542 eV exhibits stability at this temperature. O1s XPS spectra measured under the same conditions after reaction treatment followed by annealing the sample at 570 K in UHV, shows

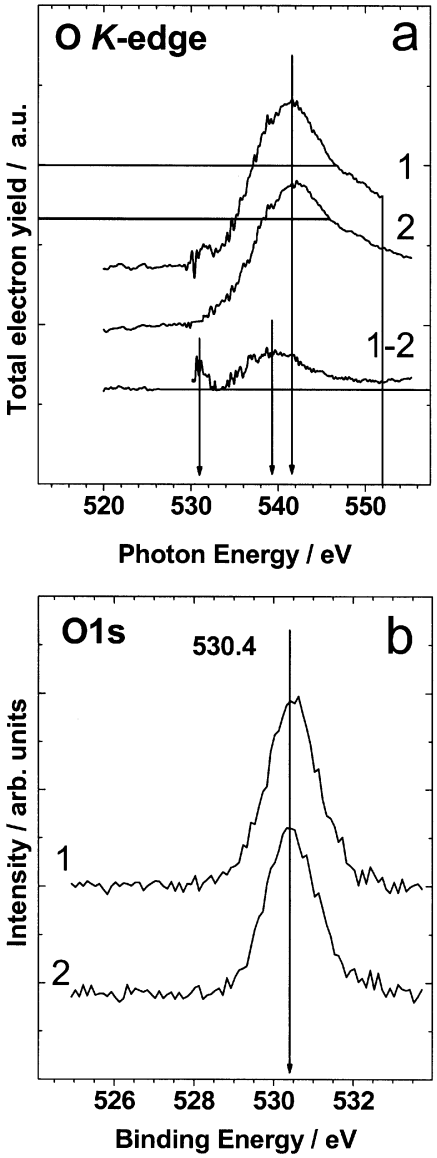

Figure 24. O K edge X-ray absorption (a) and O 1s core level photoemission (b) spectra from the silver foil pre-treated for 6 h by a C_2H_4 (2%) + O_2 reaction mixture at T = 470 K and p = 2mbar (1) followed by heating up to T = 570 K in UHV (2). Difference XAS spectrum (1–2) is also shown.

only one maximum at 530.4 eV, which might belong to at least three surface species: hydroxides, carbonates and absorbed oxygen [24, 26–28]. Even the temperature behavior does not help assigning the maximum to an oxygen species. Hydroxide and carbonates are unstable at 470 K on clean silver surfaces, but they can be stabilized by defects due to the activation of the catalyst at the severe reaction conditions used in the study. UPS spectra should demonstrate characteristic features for hydroxides and carbonates at 8.2 eV, 11.0 eV and 8.5 eV, respectively. UPS spectra measured after the same catalyst treatment did not show such structures. The He I spectrum of the silver foil is characterized by two features at 3.5 eV and 6.5 eV after activation of the catalyst at p = 2 mbar. According to the literature, these features are due to

oxygen 2p derived bands, which are anti-bonding and bonding with respect to the oxygen-silver bond [29]. This oxygen species, which is also identified in previous papers, is called electrophilic oxygen [22, 26].

The small peak observed in the ex situ O K edge X-ray absorption spectrum of the foil after reaction treatment at 531 eV is assigned to nucleophilic oxygen (Ag_2O) since the structure disappears after heating to 570 K in vacuum [24, 27]. This temperature coincides with the decomposition temperature of nucleophilic oxygen [24, 27]. The assignment is confirmed by the identical spectrum of a silver foil measured at T = 470 K and p = 10^{-4} mbar oxygen, measured by the same authors in a previous study [30]. These conditions are known to be sufficient for the formation of the oxide-like oxygen with a coverage of half a monolayer. In the O1s XPS spectrum, no indication for nucleophilic oxygen was found. The reason might be the high amount of hydrocarbons in the rest of the gas of the UHV-chamber, which was used for XPS measurements, since this chamber was pumped by a diffusion pump. Nucleophilic oxygen is known to be removed by reaction with hydrocarbons. The presented *in-situ* XAS measurements were performed in a hydrocarbon free chamber pumped by turbomolecular pumps. The authors compared the O K edge spectrum of electrophilic oxygen with the spectra of molecularly chemisorbed oxygen on Ag(110) from a XAS study of Stöhr et al. [31]. The spectra of the molecularly adsorbed oxygen are characterized by π*- and σ*-resonances. The absence of any resonances in the spectrum of the electrophilic oxygen is a strong indication for atomic character of this species.

It is remarkable that the active species in the ethylene epoxidation over silver and the active species for the methanol oxidation over copper show very similar characteristics. In both cases, the active surface is characterized by a weakly bonded atomic oxygen species, which differs clearly from the metal-oxide oxygen.

3.5. Autoreduction of Fe/ZSM5

As a further example of the application of soft X-ray metal edges, the autoreduction behavior of Fe/ZSM5 is discussed. Two Fe/ZSM5 samples that have been calcined under either mild or severe conditions will be compared [12]. The 2p X-ray absorption spectra of Fe/ZSM5 are measured and from these spectra, the average valence of iron is determined by comparing the *in-situ* detected spectral shape with reference spectra of Fe/ZSM5 in its most oxidized (Fe^{III}) and most reduced (Fe^{II}) forms, where we have assumed full oxidation and reduction, respectively. By analyzing the spectra in this way, we are able to follow the mean valence of the iron in Fe/ZSM5 during treatments at temperatures between 300 and 625 K and under gas flows of He and O_2. The relative uncertainty in the effective valence of iron is less than 0.01. Fast Fe L_3 measurements with 50-second intervals were taken in the energy range of 707 to 719 eV. Periodically, we recorded the complete Fe $L_{2,3}$ spectral shape to check variations in the background.

Fig. 25 shows the variation of the average valence as a function of time. The valence of a hard-calcined Fe/ZSM5 sample under 5% O_2 in He at room temperature first shows an oxidation to a valence of 2.94 ± 0.01 and stays constant at this value for 50 minutes. At t = 90 minutes, we switch to pure He, after which the sample reduces in 15 minutes to a

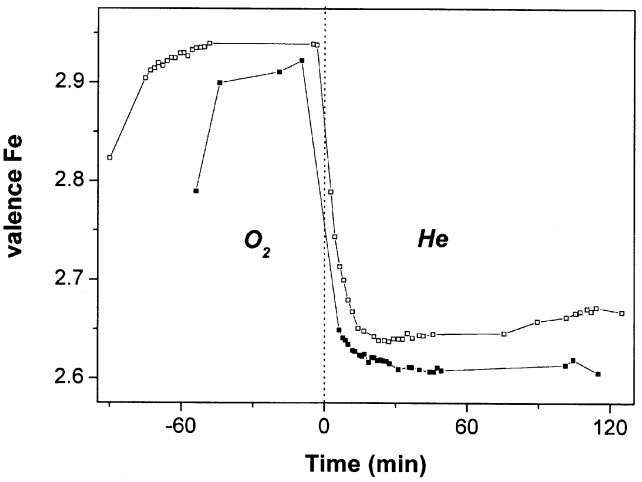

Figure 25. Oxidation of Fe/ZSM5 in O_2 (5% in He) and autoreduction in He at room temperature (mildly calcined (■), hardly calcined (□)).

minimum valence of 2.64, followed by a slight re-oxidation to a value of approximately 2.68 after 200 minutes. The mild-calcined Fe/ZSM5 has a valence of 2.91 ± 0.03 and reduces to 2.61, remaining essentially constant over more than 60 minutes. This observation indicates a dynamic local valence of the Fe/ZSM5 samples. Similar experiments have been carried out at increased temperatures up to 350°C and also under various experimental conditions. The main conclusion we would like to draw here is that from the detailed understanding of the 2p X-ray absorption spectral shapes, it is possible to obtain accurate numbers for the average iron valence that can be measured *in-situ* [12]

4. RELATED TECHNIQUES

4.1. Soft XAS Using Fluorescence Detection

Photon-in photon-out *in-situ* soft X-ray absorption measurements of catalytic reaction involving mainly hydrocarbons were shown to be possible by the development of a high-efficiency, near normal incidence focusing multilayer mirror (MLM) detection system for carbon K edge fluorescence yield [32]. Photon-in photon-out spectroscopy has been developed for *in-situ* single crystal surface science experiments involving chemisorption, displacement and dehydrogenation of carbon species [33–37]. Since the fluorescence yield of carbon is very low (~0.0012), it is crucial to increase the detection efficiency as much as possible. Simply increasing the intensity of the incident intensity might induce sample damage. Therefore, a high efficiency differentially pumped ultra-high vacuum compatible proportional counter optimized for carbon fluorescence detection was developed [38]. The detector has an overall efficiency of about 40 % and it collects about 5 % of the available solid angle from the sample. The two entrance windows of the detector are 1 μm polypropylene film and provide an effective low pass soft X-ray filter at the carbon K edge, reducing the sensitivity to higher-order-induced excitation of nitrogen and oxygen background fluorescence from mixed ele-

ment samples. The window's low pass properties produce a background carbon edge step in the absorption due to the scattered soft X-rays from the sample. This background in the fluorescence yield in absorption measurements at the carbon K edge is eliminated by using a focusing multilayer mirror (MLM) collector. Fischer et al. reported that a MLM, intercepting a large fraction of the solid angle from the sample, providing adequate reflectivity and bandpass, and focusing the collected carbon fluorescence signal to the detector. The multilayer presents a bandpass centered about the carbon fluorescence line (277 eV) narrow enough to exclude the scattered soft X-rays above the carbon edge (284 eV). This suggests an acceptable bandpass of 1 to 2 eV. Scattered X-rays from the sample are present as a single elastic peak whose peak position is tuned to the carbon K fluorescence line and whose width is representative of the bandpass of the multilayer mirror. A system described above was used to investigate the oxidation of propyne on the Pt(111) surface from conditions of coadsorbed propyne to 0.009 Torr of oxygen [34]. The analysis of temperature-programmed fluorescence yield near edge spectroscopy measurements indicates propyne adsorbs molecularly with the C_3H_4 stoichiometry at 150 K. Analysis of the π^* resonance and the corresponding C—C σ^* resonance indicates that the π system is diminished upon adsorption nearly parallel to the surface. Exact orientation determination is not possible due to the splitting of the π^* orbital upon adsorption and low signal to noise ratio. However, the angular dependence of the C≡C σ^* resonances indicate the π system is nearly parallel to the surface, with the methyl group up from the surface plane. The authors show that skeletal oxidation and hydrogenation occur simultaneously for a wide range of oxygen-rich conditions on the Pt(111) surface with an initial activation energy of 17 Kcal/mol.

This is an interesting technique, which has the potential to be applied for *in-situ* investigations of heterogeneous catalytic processes. The method is bulk sensitive. A combination with surface sensitive methods like TEY detection will allow the correlation of the electronic structure of surface and bulk. A problem of applying MLM might be the deposition of molecules on the mirror, which change its properties. This problem might occur for *in-situ* measurements only.

4.2. X-ray Raman Detection of Soft XAS

X-ray Raman scattering from core electrons of low Z materials provides an alternative to soft X-ray absorption spectroscopy when the penetrating power of hard X-rays is needed to study bulk properties or when systems under high pressure are studied. The inelastic X-ray scattering from bound electrons in low Z materials strongly resembles its corresponding soft X-ray absorption spectrum [39]. The first X-ray Raman scattering (XRS) spectra measured by using synchrotron radiation were published by Nagasawa et al. [40]. These experiments were performed with an energy resolution of typically 1 eV at 8 keV on systems like lithium, beryllium, graphite and diamond. The first extended X-ray fine structure (EXAFS) analysis was undertaken by Tohji et al. at the carbon K edge in diamond [41].

The application of X-ray Raman scattering requires the input of undulator beamlines providing a high photon flux to compensate the low scattering cross section. Since the measurements are performed in the hard energy range, the spectra reveal information about the bulk.

5. OUTLOOK

In-situ X-ray absorption spectroscopy is a powerful tool to study heterogeneous catalytic processes. It enables correlation of the catalytic activity with the electronic surface structure of a working catalyst and is, therefore, an important tool for the formulation of reaction models. However, the surface sensitivity of *in-situ* XAS in the soft energy range measured in the total electron yield mode is limited to 7–10 nm. The quality of XAS spectra measured at the C K edge is often poor, because the optical elements of the beamline are contaminated by carbon. This requires a normalization of the detected spectra with respect to the incident photon flux. This normalization might be a source of error, especially in the case of strong contamination.

X-ray photoelectron spectroscopy has advantages compared to XAS in the soft energy range. The information depth can be changed by changing the energy of the photons. Therefore, detection of depth profiles is possible. The information depth can be reduced to 0.5 nm by detecting electrons with kinetic energy of about 50 eV. Since the photon energy is fixed during a scan, the normalization with respect to the incident photon flux is less problematic.

Recent publications show, that X-ray photoelectron spectra can be measured under water atmospheres in the mbar range [42]. The growth of ice on metals and oxides was investigated by the authors. The cell in which the sample is exposed to water pressures up to a few mbar is connected via three differential pumping stages to the electron energy analyzer, allowing the analyzer to operate in the 10^{-7} mbar range. The first experiments to apply a set up like this to investigate heterogeneous catalytic processes have been performed successfully. The combination of *in-situ* XAS in the soft energy range and *in-situ* X-ray photoelectron spectroscopy enables an estimation of the unoccupied and the occupied density of states of an active catalyst surface, respectively. Therefore, the development of *in-situ* X-ray photoelectron spectroscopy as a tool for the investigation of heterogeneous catalytic processes presents a promising outlook for the future.

The common application of *in-situ* XAS in the soft and hard energy range on the same heterogeneous catalytic process will provide information concerning the interaction of the active surface and the bulk of the catalyst. This is of special interest for the estimation of the mechanism of the reaction. It requires *in-situ* XAS studies in the hard energy range at reduced pressure. A lot of activities can be expected in the field of *in-situ* X-ray (absorption) spectroscopy in the soft energy range in the future. The high surface sensitivity allows the investigation of electronic surface structure-reactivity correlations, which form the basis to formulate reaction models.

ACKNOWLEDGMENTS

For collaboration and discussions, we would like to thank Michael Hävecker, Ralf Mayer, Thomas Schedel-Niedrig, Hendrik Bluhm, Valeri Bukhtiyarov and Robert Schlögl.

REFERENCES

1. van der Eerden, A. M. J, van Bokhoven, J. A, Smith, A. D., Koningsberger, D. C, *Review of Scientific Instruments*, 71, 3260 (2000).
2. Stöhr, J, in *NEXAFS spectroscopy*, (Springer, Berlin, 1992).
3. Briggs, D., Seah, M. P., in *Practical Surface Analysis by Auger and X-ray Photoelectron Spectroscopy*, (Wiley, New York, 1983).
4. Knop-Gericke, A., Hövecker, M., Neisius, T., Schedel-Niedrig, T., *Nuclear Instruments & Methods in Physics Research A*, 406, 311 (1998).
5. Elam, W. T., Kirkland, J. P., Neiser, R. A., Wolf, P. D., *Physical Review B*, 38, 26 (1988).
6. Erbil, A., Cargill, G. S., Frahm, R., Boehme, R. F., *Physical Review B*, 37, 2450 (1988).
7. Lytle, F. W, in *Application of Synchrotronradiation*, (Gordon and Breach, New York, 1989).
8. Tröger, L., *et al.*, *Physical Review B,* 46, 3283 (1992).
9. de Groot, F. M. F., *Chemical Review*, 101, 1779 (2001).
10. de Groot, F. M. F., Fuggle, J. C., Thole, B. T., Sawatzky, G. A., *Physical Review B*, 42, 5459 (1990).
11. de Groot, F. M. F., *Journal of Electron Spectroscopy and Related Phenomena*, 67, 529 (1994).
12. Heijboer, W. M., *et al.*, *Journal of Physical Chemistry B*, submitted, (2002).
13. Hävecker, M., PhD Thesis, Fachbereich Physik der Technische Universität Berlin, (2000).
14. Grioni, M., J. Vanacker, F., Czyzyk, M. T., Fuggle, J. C., *Physical Review B*, 45, 3309 (1992).
15. Mayer, R, Hävecker, M, Knop-Gericke, A, Schlögl, R, *Catalysis Letters*, 74, 115 (2001).
16. van Bokhoven, J. A., Roelofs, J. C. A. A., de Jong, K. P., Koningsberger, D. C., *Chemistry- a European Journal*, 7, 1258 (2001).
17. Cavani, F., Trifiro, F, Vaccari, A, *Catalysis Today*, 11, 173 (1991).
18. Knop-Gericke, A., Hävecker, M., Schedel-Niedrig, T., Schlögl, R., *Topics in Catalysis*, 10, 187 (2000).
19. Mavrikakis, M., Hammar. B., Norskov, J. K., *Physical Review Letters*, 81, 2819 (1998).
20. Ramis, G., *et al.*, *Journal of Catalysis*, 157, 523 (1995).
21. Afsin, B., Davies, P. R., Pashuski, A., Roberts, M. W., *Surface Science*, 259, L724 (1991).
22. Bukhtiyarov, V. I., Boronin. A. I., Prosvirin, I. P., Savchenko, V. I., *Journal of Catalysis*, 150, 262 (1994).
23. Grant, R. B., Lambert, R. M., *Journal of Catalysis*, 92, 364 (1985).
24. van Santen, R. A., Kuipers, H. P. C. E., *Advances in Catalysis*, 35, 265 (1987).
25. Bukhtiyarov, V. I., *et al.*, *Catalysis Letters*, 74, 121 (2001).
26. Bukhtiyarov, V. I., Kaichev, V. V., Prosovirin, I. P., Podgornov, E. A., *Catalysis Letters* 57, 233 (1999).
27. Campbell, C. T., Paffett, M. T., *Surface Science*, 143, 517 (1984).
28. Carley, A. F., Davies, P. R., Roberts, M. W., Thomas, K. K., *Surface Science*, 238, L467 (1990).
29. Prince, K. C., Bradshaw, A. M., *Surface Science*, 126, 49 (1983).
30. Bukhtiyarov, V. I., *et al.*, *Nuclear Instruments & Methods in Physics Research A* 470, 302 (2001).
31. Pawela-Crew, J., Madix, R. J., Stöhr, J., *Surface Science*, 339, 23 (1995).
32. Fischer, D. A., *et al.*, *Synchrotron Radiation News,* 15, 16 (2002).
33. Chen, J. G., Fischer, D. A., Hardenburg, J. H., Hall, R. B., *Surface Science*, 279, 13 (1992).
34. Gabelnick, A. M., Burnett. D. J., Gland, J. L., Fischer, D. A., *Journal of Physical Chemistry B*, 105, 7748 (2001).
35. Gland, J., Fischer, D. A., Zaera, F., Shen, S., *Journal of Chemical Physics*, 89, 590 (1988).
36. Gland, J. L., Rufael, T., Fischer, D. A., in *Surface Science of Catalysis: In-situ probes and reaction kinetics*, (ACS Books, New York, 1992).
37. Huang, S. X., Fischer, D. A., Gland, J. L., in *Hydrotreating technology for pollution control*, (Marcel Dekker Inc., New York, 1996).
38. Fischer, D. A., Colbert, J., Gland, J. L., *Review of Scientific Instruments*, 60, 1596 (1989).
39. Das Gupta, K., *Physical Review*, 128, 1962 (1962).
40. Nagasawa, H., Mourikis, S., Schülke, W., *Journal of the Physical Society of Japan*, 58, 710 (1989).
41. Tohji, K., *et al.*, *Journal of Chemical Physics*, 92, 3233 (1990).
42. Ogletree, D. F., *et al.*, *Review of Scientific Instruments*, 73, 3872 (2002).
43. Bluhm, H., Ogletree, D.F., Fadley, Ch., Hussain, Z., Salmeron, M., *J. Phys: Codens. Matter*, 14, L227 (2002).
44. Knop-Gericke, A., Hävecker, M., Schedel-Niedrig, T., Schlögl, R., *Topics in Catalysis*, 15, 27 (2001).
45. Mayer, R., Fachbereich Chemie, Biologie, Pharmazie der Freien Universität Berlin, (2002).